Minimum Variance Brain Source Localization for Short Data Sequences

Maryam Ravan, *Senior Member, IEEE,* James P. Reilly, *Member, IEEE,* and Gary Hasey

***Abstract*—In the electroencephalogram (EEG) or magneto-encephalogram (MEG) context, brain source localization methods that rely on estimating second order statistics often fail when the number of samples of the recorded data sequences is small in comparison to the number of electrodes. This condition is particularly relevant when measuring evoked potentials. Due to the correlated background EEG/MEG signal, an adaptive approach to localization is desirable. Previous work has addressed these issues by reducing the adaptive degrees of freedom (DoFs). This reduction results in decreased resolution and accuracy of the estimated source configuration. This paper develops and tests a new multistage adaptive processing technique based on the minimum variance beamformer for brain source localization that has been previously used in the radar statistical signal processing context. This processing, referred to as the fast fully adaptive (FFA) approach, can significantly reduce the required sample support, while still preserving all available DoFs. To demonstrate the performance of the FFA approach in the limited data scenario, simulation and experimental results are compared with two previous beamforming approaches; *i.e.*, the fully adaptive minimum variance beamforming (MVB) [8] method and the Beamspace beamforming method [18]-[20]. Both simulation and experimental results demonstrate that the FFA method can localize all types of brain activity more accurately than the other approaches with limited data.**

***Index Terms*— Electroencephalogram, magnetoencephalogram, brain source localization, beamforming, evoked potentials, fast fully adaptive processing.**

I. Introduction

Estimating the locations of sources of electrical activity in the brain is an important problem in electro- and magneto-encephalography (EEG and MEG). A large variety of algorithms have been developed for solving the EEG/MEG source localization problem, including multiple signal classification (MUSIC) [1]-[4], FINE [5]-[7], minimum variance beamforming (MVB) [8], vector-type Borgiotti-Kaplan beamforming [9], weighted minimum norm (WMN) [10], standardized low-resolution electromagnetic tomography (sLORETA) [11]-[13], and dipole fitting [14]-[16].

M. Ravan and J. P. Reilly are with the Department of Electrical and Computer Engineering, McMaster University, Hamilton, ON, Canada. Emails: mravan@ece.mcmaster.ca and reillyj@mcmaster.ca.

G. Hasey is with the Department of Psychiatry and Behavioural Neurosciences, McMaster University, and also with Mood Disorders Program, St. Joseph's Hospital, Hamilton, ON, Canada. Email: ghasey@sympatico.ca.

The EEG/MEG source localization problem is particularly difficult because the signal-to-noise ratio (SNR) is typically very low and the noise is spatially colored and often temporally nonstationary. Further, we often encounter the situation where the number of available data samples surrounding the activity of interest is limited. Such situations are common, e.g., in the important case of measuring evoked potentials. Evoked potentials are EEG or MEG responses over various parts of the brain in response to some form of stimulus, often auditory or visual. The relevant point of concern in our case is that the evoked potential response is typically of short duration.

Localization methods that rely on estimating second order statistics of the measured data or related quantities (such as signal/noise subspaces), *e.g*., MUSIC, FINE, MVB, and maximum likelihood dipole fitting (MLDF) [16] can provide excellent performance, but require sequences of sufficient duration to accurately evaluate the second-order statistics of interest. However, in limited data scenarios, the variances of the estimated second order statistical quantities or subspaces increase and localization performance deteriorates. The data requirements for such algorithms generally increase as the number of spatial channels (or electrodes) increase. For example, to obtain a sufficiently accurate estimate of the sample covariance matrix of the data for MVB with N channels (or N degrees of freedom (DoFs)), the number of statistically independent data records should be three or more times the number of channels in order to obtain statistically stable source location estimates [8], [17]. Consequently, the potential advantages of having large numbers of spatial channels are offset by requirements for increased quantities of data.

Generally, the term 'DoF' in an adaptive context refers to the number of adaptive weights that can be adjusted to yield the desired response. However, often it is advantageous to linearly transform the observed data before processing, using e.g., the Fourier or Karhunen-Loeve (KL) transforms. The adaptation process is then performed using these transformed quantities. In general the transformation preserves the number of available DoFs. However, in the *beamspace* approach, e.g., [18]-[20], which uses the KL transform, the transformation procedure has the advantage that typically, all but a few of the KL coefficients (the principal component coefficients) have negligible powers, and hence can be neglected, thereby reducing the number of DoFs. Another similar approach is *partial adaptivity*, e.g., [21], in which the number of adaptive DoFs is reduced to meet the constraints on available data. Reducing the number of DoFs yields corresponding reductions in the required sample support and computation load but at the

cost of reduced performance and focal brain activity discrimination.

An alternative approach is the proposed Fast Fully Adaptive (FFA) method that exploits all available degrees of freedom while simultaneously reducing computational complexity and the required sample support. This method has previously been used in the radar context for detecting targets buried in clutter using measured high frequency surface wave radar data with uniform linear antenna arrays [22], [23]. The term "*adaptive*" in this context suggests that the beamformer response is constrained to unity in a desired direction, yet the total output power from other directions is minimized on an adaptive basis, depending on the directional structure of the interfering background. The term "*fully adaptive*" means that all available DoFs are used in the adaptive process.

The proposed multistage adaptive processing technique draws its inspiration from the butterfly structure of the Fast Fourier Transform (FFT). Essentially, the FFA approach sub-divides the *N* channels (sensors) into groups of several channels of smaller dimension, and then uses the fully adaptive approach within each group to compute an intermediate statistic. The key idea underlying the FFA approach is that the *outputs* from each stage form the input data matrix of the subsequent stage. This process of partitioning the newly formed data matrix, followed by adaptively processing each resulting partition, is repeated until the original $N\times 1$ dimensional (channel) data matrix is reduced to a single final output whose magnitude can be compared against a chosen threshold to determine if there is any activity at the location and time under test. Hence, as with the FFT algorithm, the FFA achieves lower complexity via a divide-and-conquer approach. A distinct advantage of the FFA approach over previous conventional low-complexity beamforming methods, such as the Beamspace approach [20], is that all the adaptive DoFs are used at every stage.

In this paper we design an FFA method for localizing brain sources from an EEG signal. The extension of the FFA method from the radar case to the brain source localization case is not straightforward. The latter involves a 3-dimensional moment vector for each source whereas in the radar case, the target is indicated with a scalar function of time and location. The extension of the method to the 3-dimensional case requires modification of both the constraint equation and the partitioning procedure. The performance of this method is then evaluated, by comparisons with the MVB and Beamspace approaches using both simulated and experimental data. As the results show, the performance of the FFA method compares favorably to that of the Beamspace and MVB approaches in the "data poor" scenario, while approaching Beamspace performance in the case of larger data sets.

The remaining portion of this paper is organized as follows: Section II presents the system model and briefly reviews the fully adaptive MVB approach. Section III introduces the FFA algorithm designed for brain source localization. Section IV presents several simulation and experimental results used to evaluate the performance of the FFA and compare it with the MVB and Beamspace algorithms. Section V investigates the sensitivity of the FFA approach to the partitioning selection. Section VI concludes the paper. Analysis of the effect of the Lagrange multiplier matrices is given in the Appendix I.

II. System Model and The Adaptive MVB Concept

Here we design the FFA approach in the context of an EEG recording system with *N* electrodes. In each trial the N electrodes record the brain electrical activity over an interval of time *T* with sampling frequency f_s, so that the number of observed time samples for each trial is $K = T \times f_s$. Hence the observed data can be organized as a data matrix $\mathbf{X} \in \mathrm{R}^{N\times K}$.

Let $\mathbf{x}(k),\ k = 1, 2, ..., K$ be an $N\times 1$ vector composed of the potentials measured by the N electrodes at a given time instant *k* associated with a single dipole source. If this source has location represented by the 3×1 vector $\mathbf{q}$, then

$$\mathbf{x}(k) = \mathbf{H}(\mathbf{q})\mathbf{m}(\mathbf{q}, k), \tag{1}$$

where

$$\mathbf{m}(\mathbf{q}, k) = \alpha_{\mathbf{q}}(k)\boldsymbol{\mu}(\mathbf{q}, k), \tag{2}$$

$\alpha_{\mathbf{q}}(k)$ is a scalar function of time, which describes the variation of the moment amplitude across time, $\boldsymbol{\mu}(\mathbf{q}, k)$ is a 3×1 unit-norm vector whose elements are the *x*, *y* and *z* components of the dipole moment at time instant *k* when $\mathbf{x}$ is measured, and the columns of the $N\times 3$ lead field matrix $\mathbf{H}(\mathbf{q})$ represent solutions to the forward problem; i.e., the first column of $\mathbf{H}(\mathbf{q})$ gives the potential at the electrodes due to a dipole source at location $\mathbf{q}$ having unit moment in the *x* direction and zero moment in the *y* and *z* directions. Similarly, the second and third columns represent the potential due to sources with unit moment in the *y* and *z* directions, respectively.

We now briefly review the fundamental MVB beamformer. The medium is linear, so the potential at the scalp is the superposition of the potentials from many active sources. The vector $\mathbf{x}(k)$ then consists of the EEG/MEG potentials at the *N* electrodes due to active dipole sources at locations $\mathbf{q}_l$, $l = 1, 2, ..., L$, and noise at the k^{th} time instant. Therefore

$$\mathbf{x}(k) = \sum_{l=1}^{L} \mathbf{H}(\mathbf{q}_l)\mathbf{m}(\mathbf{q}_l, k) + \mathbf{v}(k), \tag{3}$$

where $\mathbf{v}(k)$ is the combined background EEG/MEG signal and instrumentation noise at time *k*.

A linear MVB processor produces an output $\mathbf{y}(k)$, which focuses on a specified location $\mathbf{q}_0$, as follows

$$\mathbf{y}(k) = \mathbf{W}^{\mathrm{T}}(\mathbf{q}_0)\mathbf{x}(k), \tag{4}$$

where the weighting matrices $\mathbf{W}(\mathbf{q}_0)$ are $N\times 3$ and $\blacksquare^{\mathrm{T}}$ denotes the matrix transpose. In the MVB approach, the optimal weight matrix is the one that minimizes the output variance, *i.e.*

$$\min_{\mathbf{W}(\mathbf{q}_0)} \mathrm{tr}(\mathbf{R}_{\mathrm{y}}) = \min_{\mathbf{W}(\mathbf{q}_0)} \mathrm{tr}\left[\mathbf{W}(\mathbf{q}_0)^{\mathrm{T}}\mathbf{R}_{\mathrm{x}}\mathbf{W}(\mathbf{q}_0)\right] \tag{5}$$

under the constraint,

$$\mathbf{W}^{\mathrm{T}}(\mathbf{q}_0)\mathbf{H}(\mathbf{q}_0)=\mathbf{I}\,, \tag{6}$$

where $\mathbf{R}_{\mathbf{x}}$ is the covariance matrix of the background EEG/MEG dara, $\mathbf{R}_{\mathbf{x}}=\mathrm{E}(\mathbf{v}\mathbf{v}^{\mathrm{T}})$. By adding the constraint (6) as a Lagrangian term to (5), the minimization problem becomes

$$\min_{\mathbf{W}(\mathbf{q}_0)} \mathrm{tr}\Big[\mathbf{W}(\mathbf{q}_0)^{\mathrm{T}}\mathbf{R}_x\mathbf{W}(\mathbf{q}_0)+(\mathbf{I}-\mathbf{W}(\mathbf{q}_0)^{\mathrm{T}}\mathbf{H})2\mathbf{\Lambda}\Big]\,, \tag{7}$$

where $2\mathbf{\Lambda}$ is the 3×3 matrix of Lagrange multipliers. This yields the solution

$$\mathbf{W}(\mathbf{q}_0)=\mathbf{R}_{\mathbf{x}}^{-1}\mathbf{H}(\mathbf{q}_0)\mathbf{\Lambda}\,. \tag{8}$$

In order to preserve the constraint (6) and consequently the amplitude of the source $\alpha_{\mathbf{q}_0}$ in (2) , the Lagrange multiplier matrix is obtained by substituting (8) into (6) as follows,

$$\mathbf{\Lambda}=(\mathbf{H}^{\mathrm{T}}(\mathbf{q}_0)\mathbf{R}_{\mathbf{x}}^{-1}\mathbf{H}(\mathbf{q}_0))^{-1}\,. \tag{9}$$

Therefore, the weight matrix is given by the expression

$$\mathbf{W}(\mathbf{q}_0)=\mathbf{R}_{\mathbf{x}}^{-1}\mathbf{H}(\mathbf{q}_0)(\mathbf{H}^{\mathrm{T}}(\mathbf{q}_0)\mathbf{R}_{\mathbf{x}}^{-1}\mathbf{H}(\mathbf{q}_0))^{-1}\,. \tag{10}$$

In practice, the matrix $\mathbf{R}_{\mathbf{x}}$ is unknown and an estimate $\hat{\mathbf{R}}$ in the case of zero mean data is formed as

$$\hat{\mathbf{R}}=\frac{1}{K}\sum_{k=1}^{K}\mathbf{x}(k)\mathbf{x}(k)^{\mathrm{T}}\quad. \tag{11}$$

Clearly the fully adaptive MVB processor assigns an adaptive weight to each of the N DoFs. Unfortunately, when the number of electrodes is large, the required support of at least $3N$ samples is rarely available, leading to the computation of an inaccurate estimate of the true interference statistics. This condition can lead to significant performance degradations of the MVB beamformer. While this degradation can be partially mitigated e.g. through the use of regularization [24], [25], the alternative FFA approach is presented as follows.

III. The Fast Fully Adaptive Approach

The common feature that the majority of low complexity adaptive algorithms share is that the total number of adaptive DoFs is reduced to meet the constraints on the available secondary data. This results in decreased source localization capability and a reduction in the accuracy of the estimated spatial patterns.

In this section we propose a multi stage adaptive processing FFA approach, which exploits all available degrees of freedom while simultaneously reducing computational complexity and the required sample support. The FFA scheme has the distinct advantage that the entire data matrix can be adaptively processed at every stage.

A. FFA Algorithm

In the previous section we reviewed the fully adaptive MVB approach, and described its disadvantage in terms of the large sample support requirement associated with computing an accurate version of $\hat{\mathbf{R}}$. To overcome this disadvantage without being forced to directly revert to a lower DoF transform domain, we adopt a divide and conquer (decimation) strategy.

An overview of the proposed method is now given. The problem is subdivided into P FFA stages as illustrated in Fig. 1. At the first stage, we partition the available N dimensional observed data vector $\mathbf{x}^1(k)$ at each time instant k into N_s^1 smaller vectors $\mathbf{x}_{n_s^1}^1(k)$, $n_s^1=1,2,..,N_s^1$ each of dimension N_1'. We then apply a fully adaptive MVB algorithm in the form of (4) on each of these partitions. The 3×1 beamformer outputs from each partition $\mathbf{y}_{n_s^1}^1$, $n_s^1=1,2,..,N_s^1$ (with a distinct component in the *x, y* and *z* directions) are then concatenated into a $3N_s^1$ vector $\mathbf{y}^1$, which becomes the input data $\mathbf{x}^2$ to the second stage. The value of p is then incremented to 2, and $\mathbf{x}^2$ is again repartitioned into N_s^2 vectors of dimension $3N_2'$. The values N_p' may be different in each stage. This procedure is repeated until the P^{th} stage which outputs a single final 3×1 vector $\mathbf{y}^P$.

Note that in each stage the background EEG interference and instrumentation noise are suppressed in each partition by the fully adaptive approach, yielding an attenuated residual noise in the subsequent processing stages. Further, since the maximum data length we deal with is reduced from N to $\max(N_{p=1}', 3N_{p=2,\ldots,P}')<N$, we have reduced the required sample support for covariance estimation from the minimum value of $3N$ to $3\max(N_{p=1}', 3N_{p=2,3,\ldots,P}')$. This also reduces the computational load associated with the evaluation of the beamformer weights $\mathbf{W}$ in (8) from $O(N^3)$ FLOPS (floating point operations) to $O((N_1')^3)$ FLOPS for p = 1 and $O((3N_p')^3)$ for p = 2, 3, .., P.

The FFA algorithm is now explained in detail. The algorithm is initialized by setting $p=0$. The initial beamformer output vector $\mathbf{y}^0$ is assigned to be the observed $N\times 1$ data vector $\mathbf{x}^1$. The value p is incremented to unity. Then $\mathbf{x}^1$ is partitioned accordingly into vectors $\mathbf{x}_{n_s^1}^1\in\mathrm{R}^{N_1'}$, $n_s^1=1,\ldots,N_s^1$. The channels and therefore the columns of the lead field matrix $\mathbf{H}$ ($\mathbf{q}$ is removed from the notation for simplicity) are also partitioned in a corresponding manner to yield the quantities $\mathbf{H}_{n_s^1}^1\in R^{N_1'\times 3}$.

The covariance matrix $\hat{\mathbf{R}}_{n_s^1}^1$ is formed for each partition from the available data $\mathbf{x}_{n_s^1}^1(k)$, k = 1, 2, …, K according to (11), and then the optimal $N_1'\times 3$ (fully adaptive) MVB weight matrix for the n_s^1 partition is formed as follows

$$\mathbf{W}_{n_s^1}^1=(\hat{\mathbf{R}}_{n_s^1}^1)^{-1}\mathbf{H}_{n_s^1}^1\mathbf{\Lambda}_{n_s^1}^1\,, \tag{12}$$

where $\mathbf{\Lambda}_{n_s^1}^1$ is the 3×3 Lagrange matrix. Next, we compute the 3×1 intermediate beamformer outputs $\mathbf{y}_{n_s^1}^1$ which are a function of *k*, and can be written in the form

$$\begin{aligned}\mathbf{y}_{n_s^1}^1(k)&=(\mathbf{W}_{n_s^1}^1)^{\mathrm{T}}\mathbf{x}_{n_s^1}^1(k)\\&=(\mathbf{W}_{n_s^1}^1)^{\mathrm{T}}\mathbf{v}_{n_s^1}^1(k)+(\mathbf{W}_{n_s^1}^1)^{\mathrm{T}}\mathbf{H}_{n_s^1}^1\mathbf{m}(k)\,.\\&=\mathbf{v}_{n_s^1}^2(k)+\mathbf{H}_{n_s^1}^2\mathbf{m}(k)\end{aligned} \tag{13}$$

where the 3×3 matrix $\mathbf{H}^2_{n_s^1}$ is

$$\mathbf{H}^2_{n_s^1} = (\mathbf{W}^1_{n_s^1})^{\mathrm{T}}\mathbf{H}^1_{n_s^1} = (\mathbf{\Lambda}^1_{n_s^1})^{\mathrm{T}}(\mathbf{H}^1_{n_s^1})^{\mathrm{T}}(\hat{\mathbf{R}}^1_{n_s^1})^{-1}\mathbf{H}^1_{n_s^1}, \tag{14}$$

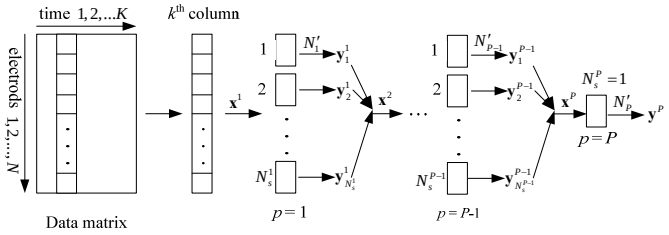

Fig. 1. The multistage representation of the FFA method. The rectangular blocks at each stage represent MVB processors.

and $\mathbf{m}(k)$ remains unchanged from the previous stage. The output vectors $\mathbf{y}^1_{n_s^1}$ at the first stage form the input vectors $\mathbf{x}^2_{n_s^1}$ at the second stage. Using (13) and (14), $\mathbf{x}^2_{n_s^1}$ can be calculated as:

$$\begin{aligned}\mathbf{x}^2_{n_s^1}(k) = \mathbf{y}^1_{n_s^1}(k) &= (\mathbf{W}^1_{n_s^1})^{\mathrm{T}}\mathbf{x}^1_{n_s^1}(k) \\ &= (\mathbf{\Lambda}^1_{n_s^1})^{\mathrm{T}}(\mathbf{H}^1_{n_s^1})^{\mathrm{T}}(\hat{\mathbf{R}}^1_{n_s^1})^{-1}\mathbf{x}^1_{n_s^1}(k)\end{aligned} \tag{15}$$

Then in the second stage we concatenate each of outputs $\mathbf{y}^1_{n_s^1}(k)$ from the first stage and the corresponding H-matrices, $\mathbf{H}^2_{n_s^1}$, into segments of length N_2'. Thus the number of segments is now $N_s^2 = N_s^1 / N_2'$. The weight matrix for the n_s^2 ($n_s^2 = 1,2,...,N_s^2$) partition of the second stage is then formed as

$$\mathbf{W}^2_{n_s^2} = (\hat{\mathbf{R}}^2_{n_s^2})^{-1}\mathbf{H}^2_{n_s^2}\mathbf{\Lambda}^2_{n_s^2} \tag{16}$$

and the subsequent output is

$$\begin{aligned}\mathbf{x}^3_{n_s^2}(k) = \mathbf{y}^2_{n_s^2}(k) &= (\mathbf{W}^2_{n_s^2})^{\mathrm{T}}\mathbf{x}^2_{n_s^2}(k) \\ &= (\mathbf{\Lambda}^2_{n_s^2})^{\mathrm{T}}(\mathbf{H}^2_{n_s^2})^{\mathrm{T}}(\hat{\mathbf{R}}^2_{n_s^2})^{-1}\mathbf{x}^2_{n_s^2}(k)\end{aligned}. \tag{17}$$

The same procedure is repeated for the stages p = 3,…, P.

It is shown in the Appendix that the output vectors $\mathbf{y}^p_{n_s^p}$ of partition n_s^p at stage p are dependent only on the Lagrange matrix $\mathbf{\Lambda}^p_{n_s^p}$ of that specific partition n_s^p, and *not* on the Lagrange matrices from other partitions at stage p, nor from any partition of the *previous* stages. As can be seen from (32) in the Appendix, this is a consequence of the fact that the Lagrange matrix $\mathbf{\Lambda}^{p-1}_{n_s^p}$ from the previous stage appears adjacent to its inverse in the expression for the output $\mathbf{y}^p_{n_s^p}$, and hence cancels out.

It follows therefore that the final output $\mathbf{y}^P = (\mathbf{W}^P)^{\mathrm{T}}\mathbf{x}^P$ from stage P is independent of all $\mathbf{\Lambda}$'s from all partitions of all previous stages (in the following, we suppress the stage and segment indexes, unless necessary). This fact has the consequence that all $\mathbf{\Lambda}$'s from all partitions of the previous stages 1, 2, …, P-1 may all be set to full rank, 3×3, but otherwise arbitrary matrices, without any impact on the value of the output from the final stage. Therefore, in the implementation of the algorithm, we set the value of the **$\mathbf{\Lambda}$'s** for stages 1, 2, …, P-1 to the identity matrix, since this is the simplest choice computationally. However, the output of the final stage P is required to be an undistorted version of the source components; therefore in this case only the constraint $\mathbf{W}^{\mathrm{T}}\mathbf{H} = \mathbf{I}$ must hold, and so the value of $\mathbf{\Lambda}$ at stage P (*i.e.* $\mathbf{\Lambda}^P$) is set according to that given by (9), with the corresponding value for $\mathbf{W}$ given by (10).

It may be seen that setting $\mathbf{\Lambda}$ in such an arbitrary manner at stages 1, 2, …, P-1 has only the effect of changing the value of the constraint equation $\mathbf{W}^{\mathrm{T}}\mathbf{H}$ in (6). To see this, we can substitute (8) into (6) to obtain

$$\mathbf{W}^{\mathrm{T}}\mathbf{H} = \mathbf{\Lambda}^{\mathrm{T}}\mathbf{H}^{\mathrm{T}}\mathbf{R}_x^{-1}\mathbf{H}. \tag{18}$$

Therefore, for arbitrary $\mathbf{\Lambda}$ we have a modified matrix as the constraint instead of the identity matrix. Notice that the $\mathbf{W}$ resulting from assigning $\mathbf{\Lambda} = \mathbf{I}$ at stages 1, 2, …, P-1 is the solution to the following modified optimization problem

$$\begin{aligned}&\min_{\mathbf{W}} \mathrm{tr}(\mathbf{R}_{\mathbf{y}}) = \min_{\mathbf{W}} \mathrm{tr}(\mathbf{W}^{\mathrm{T}}\mathbf{R}_{\mathbf{x}}\mathbf{W}) \\ &\text{subject to } \mathbf{W}^{\mathrm{T}}\mathbf{H} = \mathbf{H}^{\mathrm{T}}\mathbf{R}_x^{-1}\mathbf{H}\end{aligned}, \tag{19}$$

where the corresponding Lagrangian is given by the expression

$$\min_{\mathbf{W}} \mathrm{tr}\left[\mathbf{W}^{\mathrm{T}}\mathbf{R}_x\mathbf{W} + (\mathbf{H}^T\mathbf{R}_x^{-1}\mathbf{H} - \mathbf{W}^{\mathrm{T}}\mathbf{H})2\mathbf{\Lambda}\right]. \tag{20}$$

Therefore, the resulting optimal FFA weighting matrix in this case still minimizes output power and thus suppresses noise as in the MVB case, but under a modified constraint. The effect of this modified constraint is explained as follows. Since $\mathbf{y} = \mathbf{W}^{\mathrm{T}}\mathbf{x} = \mathbf{W}^{\mathrm{T}}\mathbf{H}\mathbf{m}$ (ignoring noise), the beamformer outputs in this case are no longer equal to the source signals as they are in the MVB case when $\mathbf{W}^{\mathrm{T}}\mathbf{H} = \mathbf{I}$; rather, they are linear combinations of the source signals whose coefficients are determined by the matrix on the right in (18). The result of the scaling operation is that the outputs are not useful entities in their own right, but this is of no consequence, since the intermediate outputs are not used for any purpose other than as inputs to the next stage.

We now discuss the case where we choose the weighting matrix $\mathbf{W}$ at stages 1, 2, …, P-1 to the MVB value given by (10), in which case the constraint $\mathbf{W}^{\mathrm{T}}\mathbf{H} = \mathbf{I}$ is in effect, with the value of $\mathbf{\Lambda}$ given by (9). Then the lead field matrix $\mathbf{H}^{p+1}$ at stage p+1 is given from (14) as $\mathbf{H}^{p+1} = (\mathbf{W}^p)^{\mathrm{T}}\mathbf{H}^p = \mathbf{I}$. This is an unusual form for the lead field matrix, and so it may appear that the spatial information in this matrix in such cases is lost. However, it may be seen that the signal component of the beamformer output resulting from this choice of weighting matrix is the source signal $\mathbf{m}(\mathbf{q})$, but with the noise component suppressed, as it is with the conventional MVB beamformer. Beamformers in subsequent stages input these source signal estimates and again output the same source signals, but with the noise component suppressed further. Thus with the preceding discussion, we see that the FFA beamformer behavior resulting from various choices of $\mathbf{\Lambda}$ indeed have sensible physical interpretations.

Regarding the fact that the beamformer input data vector $\mathbf{x}^p$ for the p^{th} stage, p = 2,…, P, is of dimension $3N_s^{p-1}$, its partitions are of dimension $3N_p'$, *i.e.*,

$\mathbf{x}_{n_s^p}^p \in \mathrm{R}^{3N_p'}$, $n_s^p = 1,\ldots,N_s^p$. Therefore, the corresponding $3N_s^{p-1} \times 3$ lead field matrix $\mathbf{H}^p$ and the MVB weight matrix $\mathbf{W}^p$ are also partitioned into the $3N_p' \times 3$ matrices $\mathbf{H}_{n_s^p}^p$, and $\mathbf{W}_{n_s^p}^p$, respectively. The introduction of directional components into the output vector $\mathbf{y}_{n_s^{p-1}}^{p-1}$ has introduced a factor of three penalty in the length of $\mathbf{x}_{n_s^p}^p$, $\mathbf{H}_{n_s^p}^p$, and $\mathbf{W}_{n_s^p}^p$ from N_p' when the source moment is a scalar, as in the radar case, to $3N_p'$ in brain source localization case. This has some adverse effects on the computational requirements of the algorithm. However, in the brain source localization application, the provision of the independent *x, y* and *z* dipole moment components is necessary to fully characterize the source, since the signals received at the electrodes will vary with the orientation of the dipole.

The advantages of the FFA are now clear: the use of the divide-and-conquer approach allows for all available DoFs to be exploited, while significantly reducing both the sample support requirements and computational load. However, it is important to note that the effective covariance matrix of the FFA scheme is a block-diagonal approximation to that of the optimal fully adaptive MVB approach. As a result, if adequate sample support were available, some performance degradation is expected. However, this degradation is mitigated by the fact that the full $N \times N$ covariance matrix estimate may be unstable in the data-poor scenario and therefore produce poorer results. An investigation of the performance of the FFA approach relative to other methods is provided in the next section.

IV. Performance Evaluation

In this section we evaluate the FFA algorithm by using both simulated and measured data.

A. Simulation Model

Here we investigate the ability of the proposed algorithm with regard to brain source localization in various scenarios, relating to the estimation of Event Related Potential (ERP) waveforms. In these simulations, the forward model (the model for determining **H**) is obtained using BrainStorm® software [26]. We use a three shell spherical head model where the *x*-, *y*- and *z*-axis are oriented along the back–front, left–right, and bottom–top direction, respectively [27], [28]. The brain radius is 9.78 cm with the center at $[x, y, z] = [1.05, -0.06, 6.11]$ cm. The conductivities of the 3 shell corresponding to the brain, skull, and scalp, were chosen to be [1, 0.0125, 1] S/m , respectively.

We use the method of [29] to generate the ERP signal. An ERP waveform exhibits a peak, which reflects phasic bursts of activity in one or more brain regions that are triggered by experimental events of interest. Specifically, it is assumed that an ERP-like waveform is evoked by each event, but that on any given trial this ERP signal is buried in background EEG noise. Thus, to improve the effective SNR, multiple ERP trials from repeated stimuli are processed to extract the ERP waveform. Typically, this processing involves only simple averaging of the multiple ERP signals.

In our application, a sequence of $N \times K$ EEG data matrices $\mathbf{X}(r)$, $r = 1, 2, ..., R$ where R is the number of ERP trials, are observed. The signal (i.e., the ERP waveform) and the background EEG noise components, are constructed using the following computational steps:

1) The peak location $\tilde{k}_r$ of the r^{th} ERP trial in time is computed by adding a normally distributed random jitter, τ_r, with a standard deviation of T_j to the mean location $\bar{k}$ of the ERP peak,

$$\tilde{k}_r = \bar{k} + \tau_r . \tag{21}$$

Then the signal component for trial *r* consists of a half cycle of a sinusoid with a user-specified frequency $\tilde{f}$ centered at peak location $\tilde{k}_r$.

2) Using the values $\tilde{k}_r$, the sampling frequency f_s and the peak frequency $\tilde{f}$, the time variation of the signal component $\mathbf{s}_{r,\mathbf{q}}$ for trial *r* and a single source *q* is calculated as follows

$$s_{r,\mathbf{q}}(k) = \begin{cases} \cos(\phi_r(k)) & if\ -\pi/2 < \phi_r < \pi/2 \\ 0 & otherwise \end{cases}, \tag{22}$$

k = 1, 2, …, *K*, where the phase ϕ_r of the signal component is given by

$$\phi_r(k) = \frac{2\pi \tilde{f}(k - \tilde{k}_r)}{f_s} \tag{23}$$

3) The noise component, $\upsilon_{r,n}(k)$ on the n^{th} channel at the r^{th} trial is taken to be a summation of 50 sinusoidal signals with increasing frequencies, $f_i = f_{i-1} + f_{rand}$, $i = 1, 2, ..., 50$, where $f_0 = 0$ Hz and f_{rand} is a uniformly distributed random variable between 0 and 2.5. Therefore, the maximum frequency could be at most equal to $2.5 \times 50 = 125$ Hz or $f_s/2$. The amplitude of the sinusoids decreases exponentially with frequency. The noise component is therefore chosen as

$$\upsilon_{r,n}(k) = \sum_{i=1}^{50} A_{f_i} \sin\left(\frac{2\pi k f_i}{f_s} + \phi_{n,i}\right), \quad \text{where} \quad A_{f_i} = \exp(-\lfloor f_i \rfloor / 25) \tag{24}$$

and $\phi_{n,i}$ is a random phase uniformly distributed over 0 to 2π radians and $\lfloor f_i \rfloor$ is the frequency f_i of the i^{th} sinusoid rounded down to the nearest integer.

4) Combining these expressions for the signal and noise terms together, the simulated $N \times K$ data matrix $\mathbf{X}_{sim}$, obtained by averaging over *R* trials, is given by

$$\mathbf{X}_{sim} = \frac{1}{R}\sum_{r=1}^{R}\left(\sum_{l=1}^{L}\mathbf{H}(\mathbf{q}_l)(\mathbf{M}(\mathbf{q}_l) \circ \mathbf{s}_{r,q_l}) + \mathbf{V}_r\right), \tag{25}$$

where $\mathbf{M}(\mathbf{q}_l) = [\boldsymbol{\mu}(q_l,1), \boldsymbol{\mu}(q_l,2), ..., \boldsymbol{\mu}(q_l,K)]$ is the $3 \times K$ matrix of unit-norm moment vectors $\boldsymbol{\mu}$ of the l^{th} source over *K* time samples, $\mathbf{s}_{r,\mathbf{q}_l} = [s_{r,\mathbf{q}_l}(1), s_{r,\mathbf{q}_l}(2), ..., s_{r,\mathbf{q}_l}(K)]$ is the row vector of signal components of the l^{th} source over *K* time samples at the r^{th} ERP trial, $\circ$ denotes component-wise multiplication, and $\mathbf{V}_r$ is the $N \times K$

matrix of noise values (from (24)) at the r^{th} ERP trial. Comparing the k^{th} column of (25) with (2) and (3), one can conclude that

$$\begin{aligned} \alpha_{\mathbf{q}_i}(k) &= \sum_{r=1}^{R} s_{r,\mathbf{q}_i}(k) / R \\ \mathbf{v}(k) &= \sum_{r=1}^{R} \mathbf{V}_r(:,k) / R \end{aligned}, \tag{26}$$

where Matlab colon notation has been used.

Here we use a HydroCel Geodesic Sensor Net (HCGSN) with $N = 256$ channels. The head model contains 6201 voxels, with a resolution of 5 mm on a side as candidate dipole locations, uniformly distributed throughout the gray matter volume of the brain. The solution space is not restricted to the cortex, so that sources from deeper structures can also contribute to the scalp EEG. We compare our proposed FFA approach with the MVB approach with regularization, the MVB approach with a large number (1000) of time samples, as well as with the Beamspace approach, with four different dipole configuration scenarios. In all cases, we generate $R = 200$ trials of ERP data with a sampling frequency of $f_s = 250$ Hz, where each trial has a length of $K = 100$ samples, corresponding to a time sequence which may be denoted using Matlab notation as [0: 4: 396] ms. The center $\bar{k}$ of the ERP peak is located at the 31st time sample (120 ms) with a jitter standard deviation of $T_j = 5$ ms across all trials, and a peak frequency value of $\tilde{f} = 10$ Hz. We assigned the value $P = 6$, with a corresponding sequence of N'_p, $p = 1, 2, .., P$, -values empirically determined as $[8, 2, 2, 2, 2, 2]$ in such a way that each partition contains clusters of neighboring sensors on the scalp. This tends to reduce the cross-correlation between the sensors' output in different partitions. For the MVB approach with regularization, we first calculate the eigen-decomposition of the covariance matrix $\hat{\mathbf{R}}$ in (11) as

$$\hat{\mathbf{R}} = \mathbf{V}\boldsymbol{\Psi}\mathbf{V}^{\mathrm{T}}. \tag{27}$$

where $\boldsymbol{\Psi}$ is the diagonal matrix of the covariance eigenvalues and $\mathbf{V}$ is the matrix of corresponding eigenvectors. Then the inverse of the covariance matrix is approximated by

$$\hat{\mathbf{R}}^{-1} \approx \mathbf{V}\hat{\boldsymbol{\Psi}}^{-1}\mathbf{V}^{\mathrm{T}}, \tag{28}$$

where $\hat{\boldsymbol{\Psi}}^{-1} = (\boldsymbol{\Psi} + \boldsymbol{\Gamma})^{-1}$, $\boldsymbol{\Gamma} = \beta\mathbf{I}$, β is the regularization parameter, and $\mathbf{I}$ is the identity matrix. The optimal value of the regularization parameter is usually determined by ad hoc methods in practical problems and there are several studies such as [25] in this area. In this study β is set to $0.005\psi_1$ where ψ_1 is the largest eigenvalue of $\hat{\mathbf{R}}$.

Since $\max(N'_{p=1}, 3N'_{p=2,\ldots,P}) = N'_{p=1}$ (first stage), the maximum number of time samples needed for calculating the covariance matrix of different stages is at least $3 \times N'_{p=1} = 3 \times 8 = 24$, which is about one fourth of the number of available time samples, which is $K = 100$.

B. Comparative Performance Evaluations

Based on the model described in the previous sub-section, we evaluate the performance of the FFA method relative to other well-known brain source localization algorithms, for the following scenarios:

1. Single cortical source: For this simulation, a single current dipole source used to generate the measured scalp voltages of the EEG electrodes was located over the left post central gyrus with coordinates $[x, y, z] = [0.603, 6.472, 8.305]$ cm. The x, y, and z components of the corresponding dipole moment are respectively, $[\mu_x, \mu_y, \mu_z] = [1, 0, 0]$. The observed data are then generated with an ERP-to-background EEG power ratio of 8 dB. The averaged signals over the 200 trials from the 256 electrodes and the corresponding topography are shown in Figs. 2 (a) and (b), respectively. The corresponding source localization results (spatial spectra) for various methods are shown in Fig.3. Both the FFA and Beamspace methods produce one peak at the same location of the source. The maximum magnitudes of the FFA and Beamspace peaks are 16.45 and 12.10 respectively, compared to the MVB value of 20.25 using 1000 time samples. The MVB method with regularization shows a localization error of 1.7 cm. The reason for this behavior is the lack of a sufficient independent data samples needed for calculating the covariance matrix accurately. The same scenario is repeated for the MVB method when 1000 data samples are used. The result is shown in Fig.3 (d). As the figure shows, with sufficient data, the MVB approach can faithfully detect the location of the source although more diffused.

2. Multiple cortical sources: The simulated EEG data in this case are produced by the activation of two spatially uncorrelated sources, located over the left middle frontal gyrus and left post central gyrus, with coordinates $[x, y, z] = [5.355, 4.774, 8.715]$ cm and $[x, y, z] = [0.603, 6.472, 8.305]$ cm, respectively. Localization results for the various methods are represented in Fig. 4. As may be observed, the FFA approach has the most concentrated spectrum, with the estimated source locations being positioned within the true source voxels. The second most accurate method is MVB with 1000 samples that estimates the locations accurately, but shows more spread around the left middle frontal gyrus source. The third method is the Beamspace approach, with a localization error of 1.43 cm for the left middle frontal gyrus source. The regularized MVB fails to discriminate the two sources and shows dispersed spatial activity between the two active locations.

3.Subcortical sources: One of the problems in source localization is depth biasing: underestimation of deep sources in favor of more superficial ones, leading to solutions that are closer to the sensors [30]. To compare the performance of methods regarding the problem with depth biasing, an EEG data set is produced by the activation of two sources located at the thalamus and the parietal right pole. The coordinates of the sources are $[x, y, z] = [-0.448, 0.709, 8.546]$ cm and $[x, y, z] = [-4.481, -2.123, 10.606]$ cm, respectively. The brain source spectra corresponding to three methods are shown in Fig. 5, where the detected locations have been mapped into MRI images. It is seen that the regularized MVB approach is unable to recover both sources whereas the FFA,

Beamspace, and MVB with 1000 samples give accurate estimates in this scenario.

4. Distributed sources: A distributed source is simulated over the left pre central gyrus with center coordinates given by $[x, y, z] = [2.5442, 5.3583, 8.0702]$ cm. The spatial variation of the sources is given by a Gaussian distribution centered within 2 cm from the center coordinate. 38 spike-like sources with a radial dipole orientation are used for the simulation. The orientation of each spike is approximated by a vector between the brain coordinate origin and the spike position [31]. The corresponding localization results are shown in Fig. 6. The FFA and Beamspace methods show more accurate results. The distribution of the FFA estimate corresponds most closely to the actual source distribution (Fig. 6(a)) with a mean squared error (MSE) of 1.09, compared to a value 2.30 for the Beamspace approach. The MVB approach with 1000 samples has an MSE of 3.2 while the regularized MVB approach shows an excessively dispersed spectrum around the source center.

5. *Joint Temporal and Spatial Processing*: To further investigate the performance of the FFA algorithm, we evaluate its performance when a single spike is injected at a particular

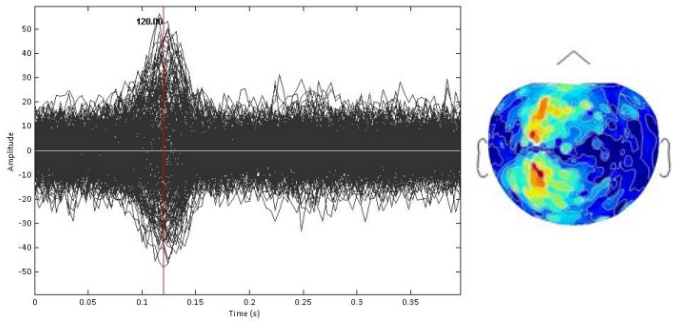

Fig. 2. Signals from 256 electrodes for the single cortical source case shown superimposed. Each trace is the average over R=200 trials (the red line indicates the center location of the ERP peak), (b) the corresponding topography.

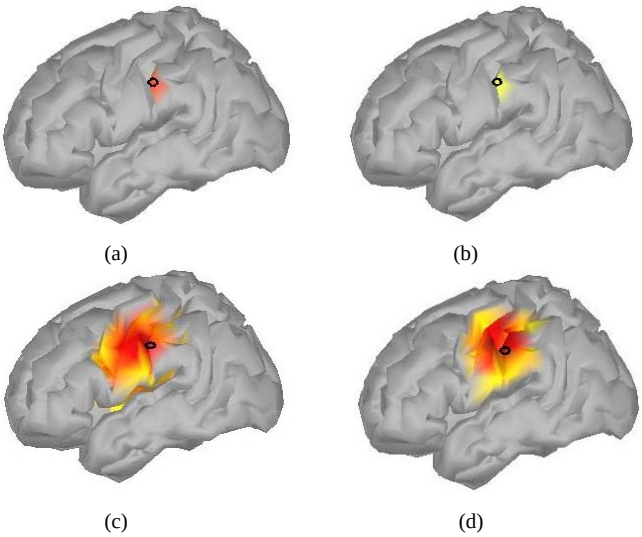

Fig. 3. Localization results of (a) FFA, (b) Beamspace, (c) MVB with regularization, and (d) MVB with 1000 time samples, when the simulated EEG data is produced by activation of a single cortical dipole located over the left post central gyrus. The black circle shows the exact location of the source.

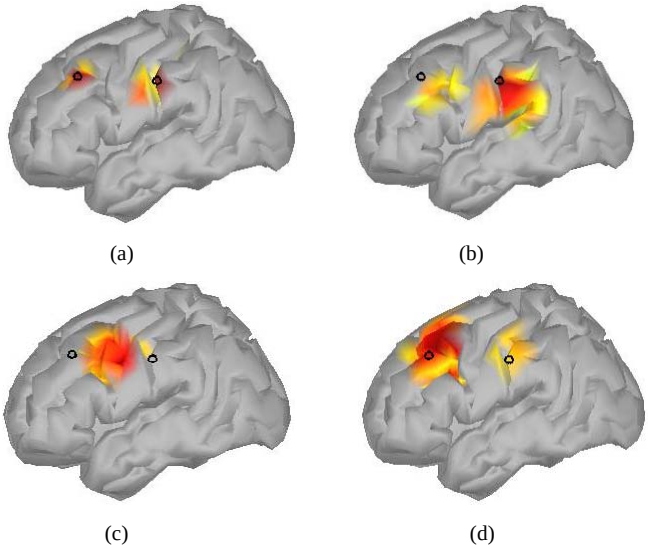

Fig. 4. Localization results of (a) FFA, (b) Beamspace, (c) MVB with regularization, and (d) MVB with 1000 time samples, when the simulated EEG data is produced by the activation of two cortical dipoles located at the left middle frontal gyrus and left post central gyrus. The black circles show the exact locations of the sources.

location of a brain at a specific time instant. The performance for this scenario is evaluated using 1000 individual simulations, where in each simulation we replace the signal component $s_{r,q}(k)$ in (22) with a spike, situated at a randomly-determined location and time. In each simulation, the signal component is based on averaging over R = 200 ERP trials, where the location and time remain fixed. The random location and time values of the spike are varied across simulation. The spike is injected with a SNR value of 10 dB, after averaging. The objective is to accurately locate both the location and time of the injected spike at each simulation. Figure 7 presents the percentages of the 1000 locations (over the entire brain volume) that are localized within 1 cm of the true location and within the 8 ms (2 time samples) of the true time instance, as a function of the number of time samples, for the FFA, Beamspace, and MVB algorithms. This procedure measures localization consistency for each method across different locations and time values. The results for the MVB approach between 50-300 samples are not computed because the estimated covariance matrix is singular in this region (and thus is not invertible) and the performance of this method cannot be evaluated. It is evident from the figure that the performance of the FFA and Beamspace methods is significantly improved over that of the conventional MVB approach for moderate to low data lengths.

6. *Results Using Real MEG Data:* In order to evaluate the performance of the algorithm in dealing with real experimental data, we use a dataset that is available from the BrainStorm toolbox [26]. This dataset originates from a somatotopy experiment recorded with a CTF MEG system (151 axial gradiometers), at La Salpetriere Hospital, Paris, where shuffled electrical stimulations are applied to the right

thumb and fingers. The data file contains the averages from 400 trials recorded from 150 MEG electrodes. In this case, we utilize an alternate head model for this dataset, referred to as

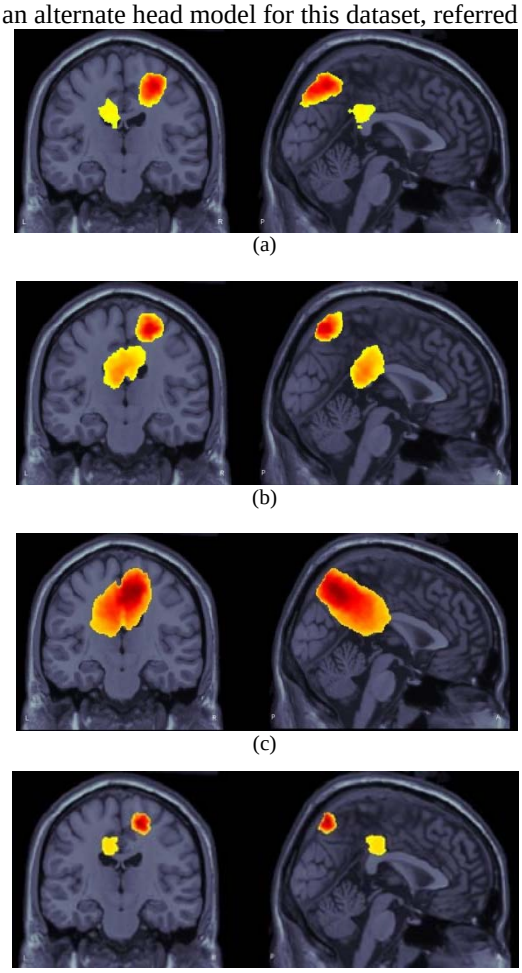

(a) (b) (c) (d)

Fig. 5. Localization results of (a) FFA, (b) Beamspace, (c) MVB with regularization, and (d) MVB with 1000 time samples mapped into MRI images, when EEG data is generated by the activation of two dipoles located at the thalamus and right parietal pole.

"overlapped spheres", that is available from the BrainStorm toolbox. This model is based on the estimation of a different sphere for each sensor; i.e., instead of using only one sphere for the whole head, it estimates a sphere that locally fits the shape of the head in the neighborhood of each sensor. This is a commonly-used approach for brain source localization. This form of model is used in this example, since it demonstrates a case where the FFA method has an advantage in terms of performance over all other methods considered in this paper. The partitioning sequence of N' values for the FFA in this case is [10, 5, 3], which requires a time sequence of at least $3\times3\times5=45$ samples in duration.

Figure. 8 shows the superimposed waveforms from each of the 150 electrodes of the measured data. Each trace is averaged over 400 Event Related Field (ERF) trials. The data is recorded over an interval which extends from 49.6 ms before the electric stimulation to 249.6 ms afterwards, with a sampling rate of 1250 Hz. Therefore, the number of available time samples is 375 per trial. As can be seen, the ERF peak occurs at a value of approximately 47.2 ms after the stimulus is applied (at time zero). Figure 9 shows the most active area of the cortex 47.2 ms after an electric stimulation of the right

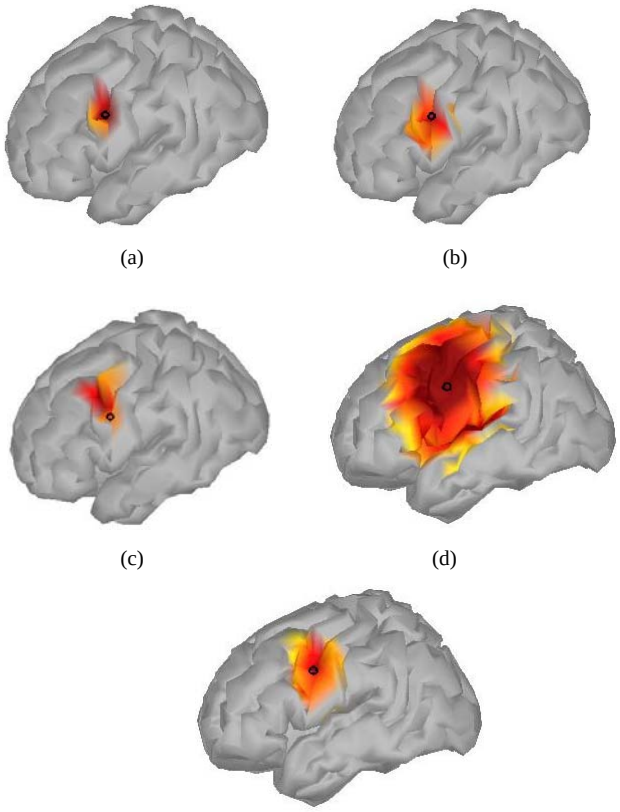

(a) (b) (c) (d) (e)

Fig. 6. (a) The actual source distribution, and localization results of (b) FFA, (c) Beamspace, (d) MVB with regularization, and (e) MVB with 1000 time samples, when EEG data is generated by the activity of a distributed source located over the left pre central gyrus. The black circle shows the center of the source.

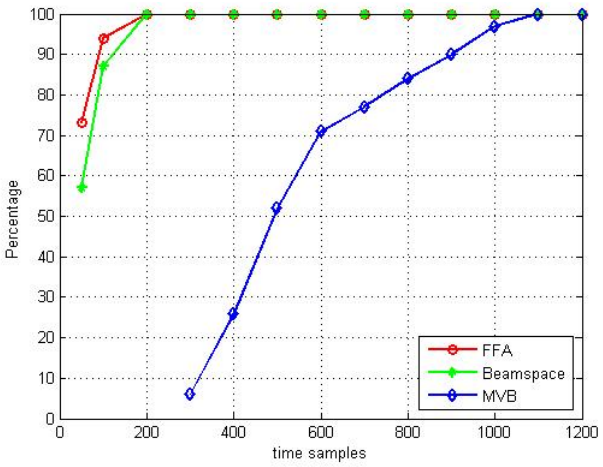

Fig. 7. Percentage of simulations for which the estimated spike source is localized within 1 cm of the true spatial location and 8 ms of the true time sample for the FFA, Beamspace, and MVB methods.

thumb. As expected, it is localized in the left hemisphere, in the middle of post central gyrus region (which is the projection of the right hand in the primary somatosensory cortex). As can be seen from the figures, the Beamspace

approach fails to estimate the active area of the brain. The reason is that the Beamspace dimension needed to obtain a normalized mean squared representation error (MSRE) of 0.1% [20] in this case was 54, while the number of available statistically independent data samples (pre-stimulus samples) in this case is just 63, which is an insufficient number for a stable covariance estimate. Furthermore, it is evident that the FFA approach again shows the most localized result. Again, the regularized MVB approach could not discriminate an active area correctly, due to the lack of sufficient statistically independent data samples.

V. FFA PARTITIONING SELECTION

The performance of the regular FFA method is characterized by two quantities; the specification of the partitioning sequence and the available sample support at each stage. As long as the number of time samples at any stage p is greater than three or more times the length N'_p of the respective partitioning sequence, then a reasonably accurate estimate of the interference covariance of each partition can be formed. However it is important to note that the choice of the partitioning sequences (as well as their ordering) can impact the performance of the FFA method.

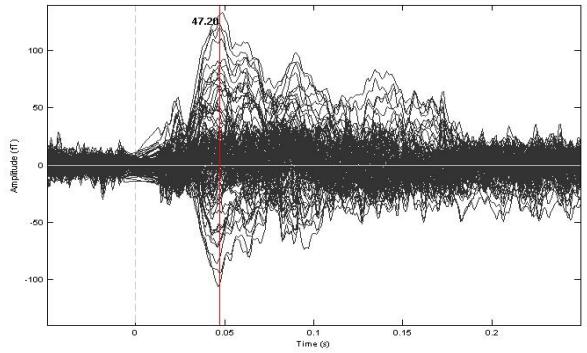

Fig. 8. Superimposed signals from the 151 electrodes used in the somatotopy experiment. The data are recorded with a CTF MEG system. Each trace has been averaged over 400 trials. The red line indicates the center location of the ERF peak.

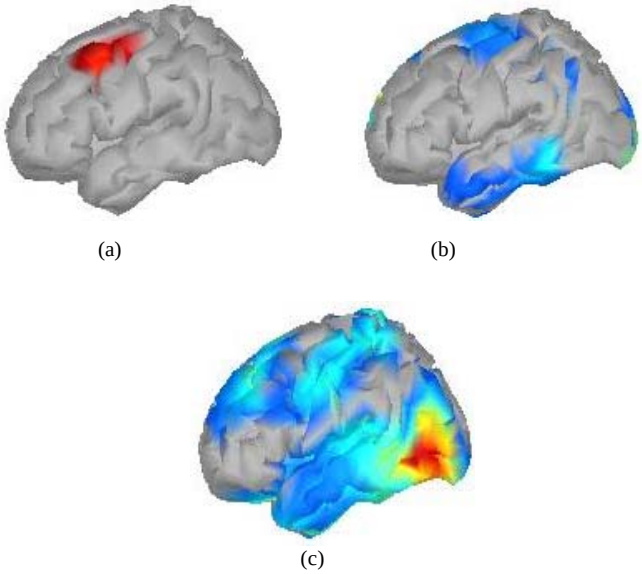

(a) (b)

(c)

Fig. 9. Localization results of (a) FFA, (b) Beamspace, and (c) MVB with regularization using data from a somatotopy experiment recorded with a CTF MEG system.

To illustrate the sensitivity of the FFA scheme to the choice of partition sequences, we performed an exhaustive search across all 112 possible partitioning sequences (that require sample support of less than 100 (available time samples)) from $[32,8]$ to $[2,2,2,2,2,2,2,2]$ for the HydroCel Geodesic Sensor Net (HCGSN) with N = 256 channels. For each partition sequence a single current dipole source (located over the left post central gyrus with coordinates $[x,y,z]=[0.603, 6.472, 8.305]$ cm (the same location as in section IV.B.1)), was used to generate the measured scalp voltages of the EEG electrodes, without any jitter and with an ERP-to-background EEG power ratio of 5 dB. We then calculated the spread radius as the distance between the true source location and the furthermost location that has amplitude of at least 70% of the source amplitude for 20 independent simulated data instances. Figure 10 (a) shows the average of the spread radius versus the partitioning sequence ranking, for all possible sequences. The sequences are ranked in ascending order of the average sequence length. It can be clearly seen from the results of this simulation that the performance of the regular FFA method is sensitive to the choice of partitioning sequences selected, with the difference between the average spread radius of the best and worst performing sequences as high as 3.21 cm. It is also worth noting that the 33 last partitioning sequences (partitioning sequences with rank 80 to 112), contain all 4 partitioning sequences that start with partitions of length 32, and 20 out of the 27 partitioning sequences that contain partitions of length 16 in their p>2 stages. This is mostly due to the limited number of time samples that prevent the accurate estimation of the covariance matrix for these cases. Figure 10 (b) plots the sample variance in spread radius computed from the 20 independent iterations for each partitioning sequence of interest. As can be seen from this plot, the variance is small for the well performing sequences and increases significantly for the badly performing sequences.

On the basis of this empirical evidence, we can suggest 1) the sequence [8,2,2,2,2,2] works well for 256 electrodes over a large range of conditions and 2) the electrodes chosen for each partition should be clusters of neighboring positions. This latter point encourages the block-diagonal FFA covariance matrix at each stage to more closely approximate the corresponding true covariance matrix at that stage.

VI. CONCLUSIONS AND DISCUSSION

In this paper a fast fully adaptive (FFA) approach is designed for brain source localization. This method uses a divide-and-conquer strategy based on the MVB method to significantly reduce the sample support requirements of the fully-adaptive scheme, and is thus particularly appropriate when measuring evoked potentials. The performance of the FFA scheme is first compared with two other localization approaches, namely Beamspace and regularized MVB, with four illustrative examples of source configuration, on a three shell spherical head model using simulated data. The simulation results show that the FFA method can localize all types of brain activities

more accurately than the other approaches. We then compare the performance of the FFA method with the Beamspace and MVB approaches by plotting the percentage of correct

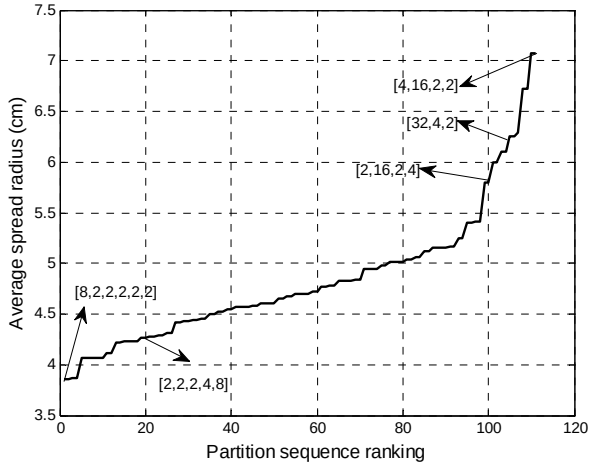

(a)

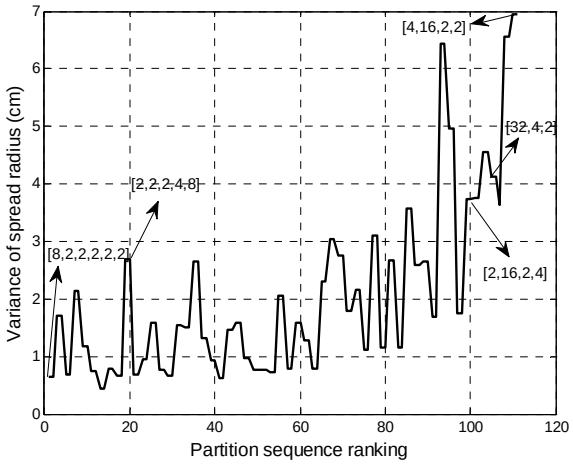

(b)

Fig. 10. (a) Average and (b) variance of the spread radius verses sequence ranking for a single current dipole source located over the left post central gyrus, for a sample support of 100 time samples.

estimation of the time and spatial locations of spike activity, versus the number of time samples, for randomly distributed source spatial and temporal locations. The FFA brain localization results show considerably improved performance in comparison to the conventional fully adaptive MVB approach in the "data poor" scenario, yet demonstrate performance that is comparable to both MVB and Beamspace in "data rich" situations.

As a final experiment, we compared the performance of the FFA method with the other two approaches using a somatotopy experiment dataset recorded with a CTF MEG system. This study showed that the spatial spectra yielded by the FFA approach were significantly more focused around the (true) active area than the Beamspace, and regularized MVB approaches. In this case, both the Beamspace and MVB approaches fail to localize activity due to the lack of statistically independent data. It is worthy of note that the improved performance of the FFA scheme arises at the cost of increased computational complexity. This is because of the multiple, although smaller, fully adaptive processes that must be executed. One could envision a parallel implementation of these processes to reduce the computational time per brain location. However, it is important to note that the FFA scheme effectively addresses the fundamental limiting factor in fully adaptive beamforming, which is the ability to accurately process a limited quantity of available training data.

The FFA approach offers choice in the selection of values of the parameters N' and N_s at each stage. Generally, the higher the value of N', the higher the resolution capabilities of the algorithm. However, a potential improvement in resolution due to a larger N' must be traded off against a higher variability in the respective covariance matrix estimates, because covariance matrices of larger dimension require more data. In turn, unstable covariance matrix estimates reduce performance. Determination of optimal values for these parameters is a difficult issue and depends greatly on the underlying environmental factors of the measurement. As such, this problem remains a topic for further investigation. In this study we formed the partitions from neighboring electrodes to reduce the cross-correlation between different partitions as much as possible.

An alternative approach, which has worked well in simulations, is to repeat the FFA algorithm for many random partitions of the data vector, and then take the average of the results. Therefore, the algorithm is not limited to any specific size of partitions, or location of sensors in the partitions. This is a topic for future research.

For ease of presentation in this paper, we have considered adaptation of the weight matrix using only a block of K samples. It is also possible to adapt the weights at every time sample, using various adaptive beamforming techniques. A very extensive literature exists on this topic. An excellent tutorial review is given in [32], and an authoritative treatment on adaptive techniques for use in the MVB context is given in [33].

It is interesting to note that the FFA approach can also be applied to other forms of MVB methods, such as the unit-noise gain method proposed by Borgiotti and Kaplan [34] and extended to the EEG/MEG case by Sekihara et al. in [9].

APPENDIX I

By concatenating the first N_2' lead field matrices $\mathbf{H}_{n_s^1}^2$ and outputs $\mathbf{x}_{n_s^1}^2$ of the first stage, $n_s^1 = 1, 2, ..., N_2'$, obtained from (14) and (15) respectively, the lead field matrices of the first segment of the second stage can be formed as

$$\mathbf{H}_1^2 = \begin{bmatrix} (\mathbf{\Lambda}_1^1)^{\mathrm{T}} (\mathbf{H}_1^1)^{\mathrm{T}} (\hat{\mathbf{R}}_1^1)^{-1} \mathbf{H}_1^1 \\ (\mathbf{\Lambda}_2^1)^{\mathrm{T}} (\mathbf{H}_2^1)^{\mathrm{T}} (\hat{\mathbf{R}}_2^1)^{-1} \mathbf{H}_2^1 \\ \vdots \\ (\mathbf{\Lambda}_{N_2'}^1)^{\mathrm{T}} (\mathbf{H}_{N_2'}^1)^{\mathrm{T}} (\hat{\mathbf{R}}_{N_2'}^1)^{-1} \mathbf{H}_{N_2'}^1 \end{bmatrix}$$

$$= \overbrace{\begin{bmatrix} (\mathbf{\Lambda}_1^1)^{\mathrm{T}} & 0 & \cdots & 0 \\ 0 & (\mathbf{\Lambda}_2^1)^{\mathrm{T}} & \cdots & 0 \\ \vdots & \vdots & \vdots & \vdots \\ 0 & 0 & \cdots & (\mathbf{\Lambda}_{N_2'}^1)^{\mathrm{T}} \end{bmatrix}}^{(\mathbf{\Lambda}^1)^{\mathrm{T}}} \overbrace{\begin{bmatrix} (\mathbf{H}_1^1)^{\mathrm{T}} (\hat{\mathbf{R}}_1^1)^{-1} \mathbf{H}_1^1 \\ (\mathbf{H}_2^1)^{\mathrm{T}} (\hat{\mathbf{R}}_2^1)^{-1} \mathbf{H}_2^1 \\ \vdots \\ (\mathbf{H}_{N_2'}^1)^{\mathrm{T}} (\hat{\mathbf{R}}_{N_2'}^1)^{-1} \mathbf{H}_{N_2'}^1 \end{bmatrix}}^{\mathbf{A}} \quad (29)$$

A similar definition applies to the remaining segments of the second stage. Notice that the two matrices $\mathbf{\Lambda}^1$ and $\mathbf{A}$ above are defined using over-arching brace-brackets. Notice in particular that the matrix $\mathbf{A}$ is independent of any value of $\mathbf{\Lambda}$. In a similar way, we can write an expression for the inputs $\mathbf{x}_1^2(k) = \mathbf{y}_1^1(k)$ to stage 2 using (4) and (8):

$$\mathbf{x}_1^2(k) = \begin{bmatrix} (\mathbf{\Lambda}_1^1)^{\mathrm{T}}(\mathbf{H}_1^1)^{\mathrm{T}}(\hat{\mathbf{R}}_1^1)^{-1}\mathbf{x}_1^1(k) \\ (\mathbf{\Lambda}_2^1)^{\mathrm{T}}(\mathbf{H}_2^1)^{\mathrm{T}}(\hat{\mathbf{R}}_2^1)^{-1}\mathbf{x}_2^1(k) \\ \vdots \\ (\mathbf{\Lambda}_{N_2'}^1)^{\mathrm{T}}(\mathbf{H}_{N_2'}^1)^{\mathrm{T}}(\hat{\mathbf{R}}_{N_2'}^1)^{-1}\mathbf{x}_{N_2'}^1(k) \end{bmatrix} = \overbrace{\begin{bmatrix} (\mathbf{\Lambda}_1^1)^{\mathrm{T}} & 0 & \cdots & 0 \\ 0 & (\mathbf{\Lambda}_2^1)^{\mathrm{T}} & \cdots & 0 \\ \vdots & \vdots & \vdots & \vdots \\ 0 & 0 & \cdots & (\mathbf{\Lambda}_{N_2'}^1)^{\mathrm{T}} \end{bmatrix}}^{(\mathbf{\Lambda}^1)^{\mathrm{T}}} \overbrace{\begin{bmatrix} (\mathbf{H}_1^1)^{\mathrm{T}}(\hat{\mathbf{R}}_1^1)^{-1}\mathbf{x}_1^1(k) \\ (\mathbf{H}_2^1)^{\mathrm{T}}(\hat{\mathbf{R}}_2^1)^{-1}\mathbf{x}_2^1(k) \\ \vdots \\ (\mathbf{H}_{N_2'}^1)^{\mathrm{T}}(\hat{\mathbf{R}}_{N_2'}^1)^{-1}\mathbf{x}_{N_2'}^1(k) \end{bmatrix}}^{\mathbf{B}(k)}, \tag{30}$$

where $\mathbf{B}(k)$ is defined as indicated. Therefore, the covariance matrix of $\mathbf{x}_1^2(k)$ can be written as

$$\hat{\mathbf{R}}_1^2 = \frac{1}{K}\sum_{k=1}^{K}\mathbf{x}_1^2(k)(\mathbf{x}_1^2(k))^{\mathrm{T}} = (\mathbf{\Lambda}^1)^{\mathrm{T}}\overbrace{(\frac{1}{K}\sum_{k=1}^{K}\mathbf{B}(k)(\mathbf{B}(k))^{\mathrm{T}})}^{\mathbf{C}}\mathbf{\Lambda}^1 \tag{31}$$

where again $\mathbf{C}$ is defined as indicated. Note that both $\mathbf{B}$ and $\mathbf{C}$ are independent of $\mathbf{\Lambda}^1$. Hence the output $\mathbf{y}_1^2(k)$ of the first segment of the second stage is given from (4) and (30) as

$$\begin{aligned} \mathbf{y}_1^2(k) &= (\mathbf{W}_1^2)^{\mathrm{T}}\mathbf{x}_1^2(k) = (\mathbf{\Lambda}_1^2)^{\mathrm{T}}(\mathbf{H}_1^2)^{\mathrm{T}}(\hat{\mathbf{R}}_1^2)^{-1}\mathbf{x}_1^2(k) \\ &= (\mathbf{\Lambda}_1^2)^{\mathrm{T}}[(\mathbf{A}^{\mathrm{T}}(\mathbf{\Lambda}^1))((\mathbf{\Lambda}^1)^{\mathrm{T}}\mathbf{C}(\mathbf{\Lambda}^1))^{-1}((\mathbf{\Lambda}^1)^{\mathrm{T}}\mathbf{B}(k))] \\ &= (\mathbf{\Lambda}_1^2)^{\mathrm{T}}[\mathbf{A}^{\mathrm{T}}(\mathbf{\Lambda}^1)(\mathbf{\Lambda}^1)^{-1}\mathbf{C}^{-1}(\mathbf{\Lambda}^1)^{-\mathrm{T}}(\mathbf{\Lambda}^1)^{\mathrm{T}}\mathbf{B}(k)] \\ &= (\mathbf{\Lambda}_1^2)^{\mathrm{T}}[\mathbf{A}^{\mathrm{T}}\mathbf{C}^{-1}\mathbf{B}(k)] \end{aligned} \tag{32}$$

where in the second line we have used both (29) and (31). Note that this expression is independent of $\mathbf{\Lambda}^1$. This same analysis applies to all segments of the second stage. Further, this treatment is trivially generalized to show that the output from stage p is independent of all the $\mathbf{\Lambda}$'s from stage p-*1*, for p=2, 3, ..., P (by replacing stage 2 with stage p and stage 1 with stage p-1). Since we have shown that $\mathbf{y}^2(k)$ is independent of $\mathbf{\Lambda}^1$ it follows by induction that $\mathbf{y}^p(k)$ is independent of the $\mathbf{\Lambda}^{p-1}, p = 2,3,..,P$. Consequently, the output $\mathbf{y}^P(k)$ at stage P depends only on the 3×3 matrix $\mathbf{\Lambda}^P$. Therefore, by choosing the constraint $\mathbf{W}^{\mathrm{T}}\mathbf{H} = \mathbf{I}$ only at stage P according to (6), we will produce an undistorted output which preserves the sources. The $\mathbf{\Lambda}$'s from previous stages, with their corresponding constraints, may be set arbitrarily as explained previously. This proves that the final output of the FFA approach does not depend on the Lagrange matrices $\mathbf{\Lambda}_{n_s^p}^p$ of segments $n_s^p = 1,2,..,N_s^p$ from stages p = 1, 2, ..., P-1.

REFERENCES

[1] J. C. Mosher, P. S. Lewis, and R. M. Leahy, "Multiple dipole modeling and localization of spatio-temporal MEG data," *IEEE Trans. Biomed. Eng.*, vol. 39, no. 6, pp. 541–557, Jun. 1992.

[2] J. C. Mosher and R. M. Leahy, "Source localization using recursively applied and projected (RAP) MUSIC," *IEEE Trans. Signal Proc.*, vol. 47, no. 2, pp. 332–340, Feb. 1999.

[3] K. Sekihara, D. Poeppel, A. Marantz, H. Koizumi, and Y. Miyashita, "Noise covariance incorporated MEG-MUSIC algorithm: a method for multiple-dipole estimation tolerant of background brain activity," *IEEE Trans. Biomed. Eng.*, vol. 44, no. 9, pp. 839–847, Sep. 1997.

[4] H. Liu and P. H. Schimpf, "Efficient localization of synchronous EEG source activities using a modified RAP-MUSIC algorithm," *IEEE Trans. Biomed. Eng.*, vol. 53, no. 4, pp. 652–661, Apr. 2006.

[5] X. L. Xu, B. Xu, and B. He, "An alternative subspace approach to EEG dipole source localization," *Phys. Med. Biol.*,vol. 49, pp. 327–343, Jan. 2004.

[6] L. Ding, G. A. Worrell, T. D. Lagerlund, and B. Hea, "Ictal source analysis: localization and imaging of causal interactions in humans," *Neuroimage*, vol. 34, no.2, pp. 575–586, Jan. 2007.

[7] Y. Lu , L. Yang, G. A. Worrell, and B. He, "Seizure source imaging by means of FINE spatio-temporal dipole localization and directed transfer function in partial epilepsy patients," *Clin Neurophysiol.*, vol. 123, no. 7, pp. 1275–1283, Jul. 2012.

[8] B. D. Van Veen, W. van Drongelen, M. Yuchtman, and A. Suzuki, "Localization of brain electrical activity via linearly constrained minimum variance spatial filtering," *IEEE Trans. Biomed. Eng.*, vol. 44, no. 9, pp. 867–880, Sep. 1997.

[9] K. S. Sekihara, S. S. Nagarajan, D. Poeppel, A. Marantz, and Y. Miyashita, "Reconstructing spatio-temporal activities of neural sources using an MEG vector beamformer technique," *IEEE Trans. Biomed. Eng.*, vol. 48, no. 7, pp. 760–771, Jul. 2001.

[10] M. Hämäläinen, R. Hari, R. J. Ilmoniemi, J. Knuutila, and O. V. Lounasmaa, "Magnetoencephalography—Theory, instrumentation, and applications to noninvasive studies of the working human brain," *Rev. Mod. Phys.*, vol. 65, no. 2, pp. 413–497, 1993.

[11] R. D. Pascual-Marqui, "Standardized low resolution brain electromagnetic tomography (sLORETA): technical details," *Meth. Findings Exp. Clin. Pharmacol.*, vol. 24, pp. 5–12, 2002.

[12] K. Rafik, B. H. Ahmed, F. Imed, T.-A. Abdelmalik, Recursive sLORETA-FOCUSS algorithm for EEG dipoles localization," in *Proc. Conf. Image Process. Theory, Tools Appl.*, pp. 1–5, Nov. 2008.

[13] C. Cao and S. Slobounov, "Alteration of cortical functional connectivity as a result of traumatic brain injury revealed by graph theory, ICA and sLORETA analyses of EEG signals," *IEEE Trans. Neural Syst. Rehabil. Eng.*, vol. 18, no. 1, pp. 11–19, Feb. 2010.

[14] M. Scherg and D. Von Cramon, "Two bilateral sources of the late AEP as indentified by a spatio-temporal dipole model," *Electroencephalogr. Clin. Neurophysiol.*, vol. 62, no. 1, pp. 32–44, Jan. 1985.

[15] S. Baillet, J. C. Mosher, and R. M. Leahy, "Electromagnetic brain mapping," *IEEE Signal Proc. Mag.*, vol. 18, no. 6, pp. 14–30, Nov. 2001.

[16] A. Dogandzic and A. Nehori, "Estimating evoked dipole responses in unknown spatially correlated noise with EEG/MEG arrays," *IEEE Trans. Signal Proc.*, vol. 48, no. 1, pp. 13–25, Jan. 2000.

[17] S. Reed, J. Mallett, and L. Brennan, "Rapid convergence rate in adaptive arrays," *IEEE Trans. Aerosp.Electron. Syst.*, vol. 10, no. 6, pp. 853–863, Nov. 1974.

[18] X. Guanghan, S. D. Silverstein, R. H. Roy, and T. Kailath, "Beamspace ESPRIT," *IEEE Trans. Signal Proc.*, vol. 42, no. 2, pp. 349–356, Feb. 1994.

[19] M. D. Zoltowski and T. S. Lee, "Maximum likelihood based sensor array signal processing in the beamspace domain for low angle radar tracking," *IEEE Trans. Signal Proc.*, vol. 39, no. 3, pp. 656–671, Mar. 1991.

[20] A. Rodríguez-Rivera, B. V. Baryshnikov, B. D. Van Veen, and R. T. Wakai, "MEG and EEG source localization in Beamspace," *IEEE Trans. Biomed. Eng.*, vol. 53, no. 3, pp. 430–441, Mar. 2006.

[21] D. J. Chapman, "Partial adaptivity for the large array," *IEEE Trans. Ant. Propag.*, vol. 24, no. 5, pp. 685–696, Sep. 1976.

[22] O. Saleh, R. S. Adve, and R. J. Riddolls, "Fast fully adaptive processing: A multistage STAP approach," in *Proc. IEEE Radar Conf.*, May 2009.

[23] M. Ravan, O. Saleh, R. S. Adve, K. Plataniotis, and P. Missailidis, "KBSTAP implementation for HFSWR," Final report for Defense Research and Development Canada, Tech. Rep. W7714-060999/001/SV, Mar. 2008, [Online] Available: http://www.comm.utoronto.ca/∼rsadve/ .

[24] A. N. Tikhonov and V. Y. Arsenin, *Solutions of Ill-Posed Problems*. New York: Wiley, 1977.

[25] M. J. Brookes, J. VRBA, S. E. Robinson, C. M. Stevenson, , A. M. Peters, G. R. Barnes, A. Hillebrand, and P. G. Morris, "Optimising experimental design for MEG beamformer imaging," *NeuroImage*, vol. 39, no. 4, pp. 1788–1802, Feb. 2008.

[26] BrainStorm, Matlab Toolbox [Online]. Available: http://neuroimage.usc.edu/brainstorm/

[27] P. Berg, and M. Scherg, "A fast method for forward computation of multiple-shell spherical head models," *Electroenceph. Clin. Neurophysiol.*, vol. 90, no. 1, pp. 58–64, Jan. 1994.

[28] J. C. Mosher, R. M. Leahy, and P. S. Lewis, "EEG and MEG: forward solutions for inverse methods," *IEEE Trans. Biomed. Eng.*, vol. 46, no. 3, pp. 245–259, Mar. 1999.

[29] N. Yeung, R. Bogacz, C. B. Holroyd, and J. D. Cohen, "Detection of synchronized oscillations in the electroencephalogram: An evaluation of methods," *Psychophysiol.*, vol. 41, pp. 822–832, 2004.

[30] G. Yildiz, A. D. Duru, and A. Ademoglu, "A comparative study of localization approaches to EEG source imaging," *IEEE NIH Life Sci. Syst. Appl.Workshop (LiSSA)*, Leuven, Belgium, pp. 156–159, Nov. 2007.

[31] M. Dümpelmann, T. Ball, and A. Schulze-Bonhage, "sLORETA allows reliable distributed source reconstruction based on subdural strip and grid recordings," *Hum. Brain Mapp.*, vol. 33, no. 5, pp. 1172–1188, May 2012.

[32] D. Van Veen and K. M. Buckley, "Beamforming: a versatile approach to spatial filtering," *IEEE ASSP Mag.*, vol.5, no.2, pp. 4–24, Apr. 1988.

[33] S. Haykin, *Adaptive Filter Theory*. 4th ed. Upper Saddle River, NJ: Prentice-Hall, 2002.

[34] G. Borgiotti and L. J. Kaplan, "Superresolution of uncorrelated interference sources by using adaptive array technique," *IEEE Trans. Ant. Propag.*, vol. 27,no. 6, pp. 842–845, Nov. 1979.